



Role of structural anisotropy in geometric birefringence of high-birefringence index-guiding PCFs: analysis by moment of inertia

Sheng Liang¹ · Yongxin Zhang¹ · Xingyu Zhang¹ · Xinzhi Sheng¹ · Shuqin Lou² · Xin Wang² · Bo Lin³ · Mingli Dong⁴ · Lianqing Zhu⁴ · Jueting Luo¹ · Rui Peng¹ · Liuyan Liang¹ · Yuqin Lin¹ · Jinli Wang¹ · Yue Yang¹ · Shuai Kang¹ · Yuelang Huang¹ · Jiazheng Ding¹ · Wenxuan Xu¹ · Fuxiao Li¹

Received: 4 June 2018 / Accepted: 6 December 2018 / Published online: 12 December 2018
© Springer Science+Business Media, LLC, part of Springer Nature 2018

Abstract

We have studied the role of structural anisotropy on the geometric birefringence of four typical high-birefringence (HB) index-guiding photonic crystal fibers (PCFs) with the same air-silica structure and circular, ellipse, and rectangle air holes, respectively. The normalized difference between the moment of inertia ΔI in x and y direction of the PCF structure is utilized to quantitatively describe the structural anisotropy. We demonstrate that the phase birefringence B increases monotonously when the normalized ΔI rises in different cases of PCFs structures. In order to obtain high birefringence B , it can be an effective method to optimize the parameters of the structure to increase the normalized ΔI . This work can be not only a reference of founding the essence of geometric birefringence and proposing the optimal design of HB-IG-PCFs, but also an enlightenment for bringing the different method (compared to the finite element) into the investigation of PCFs.

Keywords Photonic crystal fiber (PCF) · Birefringence · Polarization maintenance · Structural anisotropy · Geometric birefringence · Moment of inertia

✉ Sheng Liang
shliang@bjtu.edu.cn

¹ Key Laboratory of Education Ministry on Luminescence and Optical Information Technology, National Physical Experiment Teaching Demonstration Center, Department of Physics, School of Science, Beijing Jiaotong University, Beijing 100044, China

² School of Electronic and Information Engineering, Beijing Jiaotong University, Beijing 100044, China

³ China Academy of Electronics and Information Technology, Beijing 100041, China

⁴ Beijing Engineering Research Center of Optoelectronic Information and Instruments, Beijing Key Laboratory for Optoelectronics Measurement Technology, Beijing Information Science and Technology University, Beijing 100016, China

1 Introduction

High-birefringence (HB) optical fibers have been widely utilized in applications that require polarization maintenance (PM), such as precise interferometric fiber-optic sensors, quantum computers, atom spectroscopy, and fiber lasers and amplifiers (Habib et al. 2014a). Photonic crystal fibers (PCFs) have many unusual optical properties, including endlessly single-mode operation, large mode area, high nonlinearity, HB and tailorable chromatic dispersion, compared with conventional optical fiber (Knight 2003). Among them, HB is one of the most interesting characteristics of the PCFs (Habib et al. 2013, 2014a, b; Mousavi et al. 2016; Chen et al. 2004; Hu et al. 2009; Gangwar and Singh 2016; Liu and Lai 2005; Sun et al. 2007; Jiang et al. 2015; Habib and Khandker 2015; Chen and Shen 2007; Hasan et al. 2014; Szpulak et al. 2005; Samiul Habib et al. 2013; Song et al. 2007; Saitoh and Koshiba 2003; Yue et al. 2007; Zhang and Yang 2004; Yang et al. 2015; Xu et al. 2004; Brosi et al. 2008; Wei et al. 2014; Huang et al. 2014; Li and Zhao 2013). Therefore, HB-PCFs have been attracting great interest in the research community for HB optical fibers. HB index-guiding (IG) PCFs are far more superior for producing HB due to the higher birefringence, lower loss, and easier fabrication, compared with common fibers and other PCFs. The highest birefringence reported HB-IG-PCFS is in the order of 10^{-2} for 1550 nm operation (Habib et al. 2014a), which is limited by the refractive index contrast between the silica core and silica-air cladding. However, this is far higher than that of commercial common PM optical fibers ($\sim 10^{-4}$ for 1550 nm), and Anti-resonance (AR) PCFs ($\sim 10^{-4}$ for 1550 nm) (Mousavi et al. 2016), and easier to fabricate with lower confinement loss compared to the photonic bandgap (PBG) hollow PCFs (Maximal value of phase birefringence $\sim 10^{-2}$, however, generally $\sim 10^{-3}$ for 1550 nm) (Chen et al. 2004).

When the symmetry in PCF is affected by artificial stress or geometric defect, the degeneracy is lifted and the real parts of the effective indices n_{eff} of the degenerate modes can separate to produce a high modal birefringence. However, the geometric birefringence is more stable in the temperature fluctuation, and easier to be fabricated compared with the stress induced birefringence (Habib et al. 2013, 2014a, b; Hu et al. 2009; Gangwar and Singh 2016; Liu and Lai 2005; Sun et al. 2007; Jiang et al. 2015; Habib and Khandker 2015; Chen and Shen 2007; Hasan et al. 2014; Szpulak et al. 2005; Samiul Habib et al. 2013; Song et al. 2007; Saitoh and Koshiba 2003; Yue et al. 2007; Zhang and Yang 2004; Yang et al. 2015). Therefore, the geometric birefringence is generally the preferred method. There are many methods to induce high geometric birefringence in HB-IG-PCFs. The key point is to break the symmetry of the structure to make the effective index difference between the two orthogonal polarization states, by utilizing asymmetric (noncircular) holes, such as the elliptical core (Hu et al. 2009), elliptical (Gangwar and Singh 2016; Liu and Lai 2005; Sun et al. 2007) or rectangular (Jiang et al. 2015) air-hole cladding, variable air hole sizes (Habib and Khandker 2015), rotational hybrid cladding (Habib et al. 2014b), one or more artificial defects (Chen and Shen 2007; Habib et al. 2013; Hasan et al. 2014; Szpulak et al. 2005; Samiul Habib et al. 2013), or squeeze the lattice of air holes (Song et al. 2007; Saitoh and Koshiba 2003; Yue et al. 2007; Zhang and Yang 2004), horizontally shifted air hole in the core (Yang et al. 2015). Furthermore, high birefringence can be obtained by introducing high-refractive-index nanostructures into the core region, which increases the huge refractive-index contrast (Xu et al. 2004; Brosi et al. 2008; Wei et al. 2014; Huang et al. 2014; Li and Zhao 2013). However, these designs have problems of high cost, fabrication difficulty, and influences of embedded structure on stability.

The reported designs of HB-IG-PCFs are deduced discretely, and each design is proposed and investigated by the full-vector finite element method (FEM) based simulation and experiments, which means there is no essential connection between the different designs. Moreover, the theoretical relationship between the structure and the birefringence has not been revealed quantitatively so far.

In this paper, we propose a preliminary investigation on the role of structural anisotropy in geometric birefringence of HB-IG-PCFs, by the moment of inertia method. The comparison between the conventional FEM and our proposed method is shown in Table 1. We believe that our method will be an important reference to find how structural anisotropy produces the geometric birefringence, and to provide an unconventional tool to study the PCFs using the non-FEM method in future.

2 Structure and geometric birefringence in HB-IG-PCFs

2.1 Structure of HB-IG-PCFs

In order to investigate the role of structural anisotropy, we choose several different representative HB-IG-PCFs with only geometric birefringence by artificial defect (Habib et al. 2014a), circular and elliptical (Gangwar and Singh 2016), elliptical (Liu and Lai 2005), and rectangular air holes (Jiang et al. 2015). These designs are all with the same air-silica structure (the refractive index 1.0 and 1.45, respectively), and the same wavelength (1550 nm). These other designs with multifarious high-refractive-index nanostructures are ignored in this work.

The structures of the PCFs analyzed are converted to be a data array including the position coordinates (x , y), length in x and y , and the shapes (ellipse, rectangle, circular). The cross section of the first HB-IG-PCF (Habib et al. 2014a) is illustrated in Fig. 1, in a five rings 13×11 rectangular array, with $\Lambda = 0.8 \mu\text{m}$, $d = 0.975\Lambda$, $d_2 = 0.65\Lambda$, $d_3 = 0.775\Lambda$, where Λ is the pitch of the lattice, d , d_2 and d_3 , are the air-hole diameter of the first and outer two rings, the air-hole diameter of the second ring, and the air-hole diameter of the third ring, respectively. An artificial defect is created by omitting two air holes along the y -axis from the first ring to obtain the structural anisotropy and increase the geometric birefringence.

The cross section of the second HB-IG-PCF (Gangwar and Singh 2016) is illustrated in Fig. 2, by the combination of circular and elliptical air holes in the cladding, and two symmetric air circular holes are introduced located opposite side of the core, with $\Lambda = 2.4 \mu\text{m}$, $d_2 = 2.1 \mu\text{m}$, $c_1 = 0.75 \mu\text{m}$, $d_1 = 0.5 \mu\text{m}$, where d_2 is the diameter of two symmetric air holes, Λ is the pitch between the centers of the two air holes, c_1 and d_1 denote the radius of the elliptical air holes along the x -direction and along the y -direction, respectively.

The cross section of the third HB-IG-PCF (Liu and Lai 2005) is illustrated in Fig. 3, with the elliptical air holes in the cladding. The pitch is $\Lambda = 1 \mu\text{m}$, minor axis is $b = 0.2100 \mu\text{m}$, and major axis is $a = 0.4286 \mu\text{m}$. Then, the ellipticity can be calculated by: $e = b/a = 0.4900$, and it means that $e = 1$ indicates a circular.

The cross section of the fourth HB-IG-PCF (Jiang et al. 2015) is illustrated in Fig. 4, by the rectangular air holes arranged in a triangular lattice, with $\Lambda = 2 \mu\text{m}$, $b = 1 \mu\text{m}$, and $a = 0.6 \mu\text{m}$, where Λ is the pitch, a and b are the widths and lengths of the rectangular air hole, respectively.

Table 1 The comparison between the conventional FEM and our proposed moment of inertia method

Items	FEM	Moment of inertia method
Accuracy for calculating birefringence of PCF	Accurate for value of birefringence	Accurate for magnitude of birefringence
Computational complexity	Complicated	Simple
Results of relationship between PCF structure and birefringence	Discretely relationship by deductive method	Continuously relationship by inductive method
Purposes	To obtain accurate birefringence	To obtain essential and quantitatively relationship between PCF structure and birefringence

Fig. 1 The cross section of the 1st HB-IG-PCF with circular air holes and an artificial defect in a five rings 13×11 rectangular array (Habib et al. 2014a) ($\Lambda = 0.8 \mu\text{m}$, $d = 0.975\Lambda$, $d_2 = 0.65\Lambda$, $d_3 = 0.775\Lambda$)

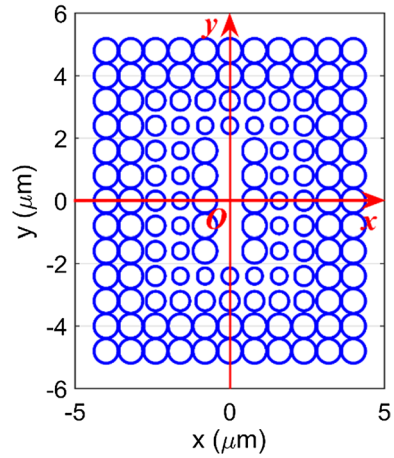


Fig. 2 The cross section of the 2nd HB-IG-PCF with circular and elliptical air holes in the cladding (Gangwar and Singh 2016) ($\Lambda = 2.4 \mu\text{m}$, $d_2 = 2.1 \mu\text{m}$, $c_1 = 0.75 \mu\text{m}$, $d_1 = 0.5 \mu\text{m}$)

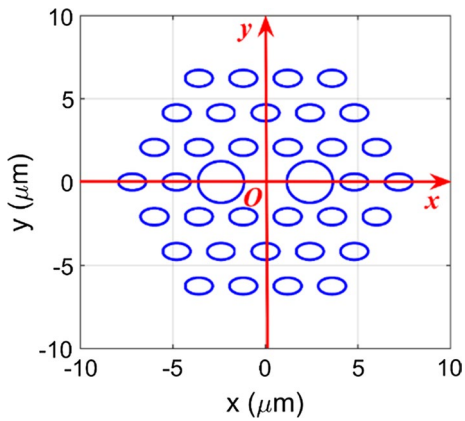
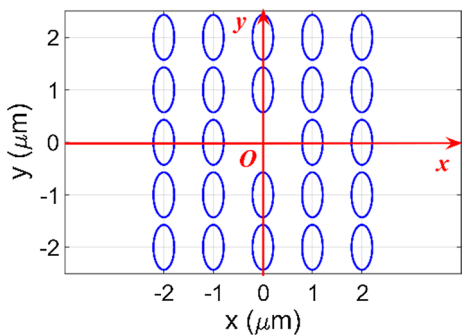


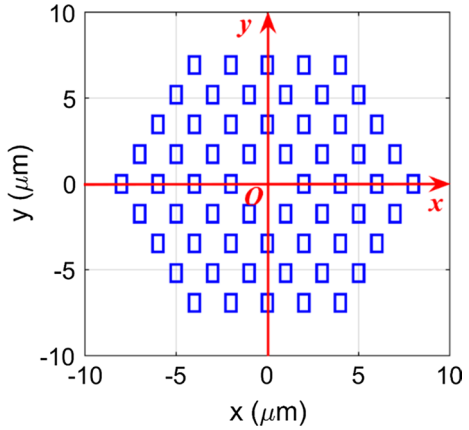
Fig. 3 The cross section of the 3rd HB-IG-PCF with the elliptical air holes in the cladding (Liu and Lai 2005) ($\Lambda = 1 \mu\text{m}$, $b = 0.2100 \mu\text{m}$, $a = 0.4286 \mu\text{m}$, and $e = b/a = 0.4900$)



The structures of the analyzed HB-IG-PCFs can be described by the vectors, and the vector V_i is for the i th air hole, as follows:

$$V_i = [x_i, y_i, L_x, L_y, S] \tag{1}$$

Fig. 4 The cross section of the 4th HB-IG-PCF with the rectangular air holes arranged in a triangular lattice (Jiang et al. 2015) ($\Lambda = 2 \mu\text{m}$, $b = 1 \mu\text{m}$, and $a = 0.6 \mu\text{m}$)



where the origin of coordinate are set at the center of HB-IG-PCFs, as shown in Figs. 1, 2, 3 and 4, L_x and L_y show the length in x and y directions (diameter for circle, the major or minor axis for elliptical, length and width for rectangle), and S is the shape of the i th air hole, respectively.

2.2 Birefringence of HB-IG-PCFs

The phase birefringence (B) or group birefringence (G), are two important parameters that characterize the highly birefringent fibers, which are defined in the following way:

$$B = \left| n_{x\text{eff}} - n_{y\text{eff}} \right| \tag{2}$$

$$G = B - \lambda \cdot dB/d\lambda \tag{3}$$

where λ is the wavelength, $n_{x\text{eff}}$ and $n_{y\text{eff}}$ are the effective indices of the x -polarized and y -polarized fundamental mode of the HB-IG-PCF.

Since the difference in value between the two parameters is usually within 10–15%, a fiber with high group birefringence also has high phase birefringence (Chen et al. 2004). In the following discussions, we only use the phase birefringence B , as the parameter for the property of HB-IG-PCFs, and the confinement loss and dispersion are ignored.

3 Moment of inertia in PCFs

It is well known that the geometric birefringence is produced by the structural anisotropy of HB-IG-PCFs, while there is no mature and effective method to quantitatively describe the structural anisotropy. The moment of inertia is a common factor to evaluate the anisotropy of an asymmetric molecule structure (Halliday et al. 2013). In this paper, we utilize the moment of inertia to describe the structural anisotropy in HB-IG-PCFs. The geometric structure of the HB-IG-PCFs is analyzed in the rectangular coordinate system as shown in Figs. 1, 2, 3 and 4, and the air holes are considered as to be the nomenclon. The moments of inertia of all air holes for axes through the centroid in the direction x and y can be expressed as:

$$I_{xx} = \sum_1^N I_{xx}(i) \tag{4}$$

$$I_{yy} = \sum_1^N I_{yy}(i) \tag{5}$$

where $I_{xx}(i)$ and $I_{yy}(i)$ are the moments of inertia of the i th air hole for axes through the centroid in the direction x and y , respectively.

For a circle, ellipse and rectangle air holes with the centroid at the coordinate (x, y) , I_{xx} and I_{yy} can be calculated by:

$$\begin{aligned} I_{xx}^{Circle} &= \pi r^4/4 + \pi r^2 y^2 \\ I_{yy}^{Circle} &= \pi r^4/4 + \pi r^2 x^2 \\ I_{xx}^{Ellipse} &= \pi r_x r_y^3/4 + \pi r_x r_y y^2 \\ I_{yy}^{Ellipse} &= \pi r_x^3 r_y/4 + \pi r_x r_y x^2 \\ I_{xx}^{Rectangle} &= L_x L_y^3/12 + L_x L_y y^2 \\ I_{yy}^{Rectangle} &= L_x^3 L_y/12 + L_x L_y x^2 \end{aligned} \tag{6}$$

where r is the radius of the circle air hole, r_x and r_y are the semi-axis length in x and y direction of the ellipse air hole, L_x and L_y are the length (or width) in x and y direction of the rectangular air hole.

In order to describe the structural anisotropy, we use the normalized difference of moments of inertia between x and y direction:

$$\Delta I = \left| I_{xx} - I_{yy} \right| / (I_{xx} + I_{yy}) \times 100\% \tag{7}$$

4 Role of structural anisotropy in geometric birefringence

For the first HB-IG-PCF illustrated in Fig. 1, when $\Lambda=0.8 \mu\text{m}$, $d=0.975\Lambda$, $d_2=0.65\Lambda$, $d_3=0.775\Lambda$, the normalized difference of moments of inertia $\Delta I_1=15.71\%$, and the phase birefringence $B_1=0.0294$ when $\lambda=1550 \text{ nm}$.

Then, for the second HB-IG-PCF illustrated in Fig. 2, the variation of the phase birefringence B with the normalized difference of moments of inertia ΔI when $d_2=2.1, 2.3, 2.5 \mu\text{m}$, $c_1=0.75 \mu\text{m}$, $d_1=0.50 \mu\text{m}$ respectively, for pitch $\Lambda=2.40 \mu\text{m}$ and $\Lambda=2.50 \mu\text{m}$, are shown in Fig. 5a, b, respectively. It is found that for both cases of $\Lambda=2.40 \mu\text{m}$ and $2.50 \mu\text{m}$, the phase birefringence B increases monotonously with ΔI .

Furthermore, for the third HB-IG-PCF illustrated in Fig. 3, the variation of the phase birefringence B and the normalized difference of moments of inertia ΔI with the ellipticity are shown in Fig. 6. Both the phase birefringence B and the normalized ΔI increase monotonously when the ellipticity rises, which means that the structural anisotropy is enhanced. As a result, it is shown that in Fig. 7, the phase birefringence B increases monotonously with the increasing of the normalized ΔI .

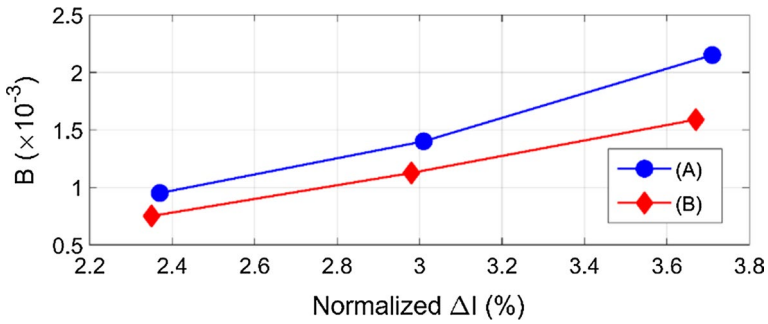


Fig. 5 Variation of B with ΔI for pitch $\Lambda=2.40$ m (a) and $\Lambda=2.50$ m (b) of 2nd HB-IG-PCF shown in Fig. 2

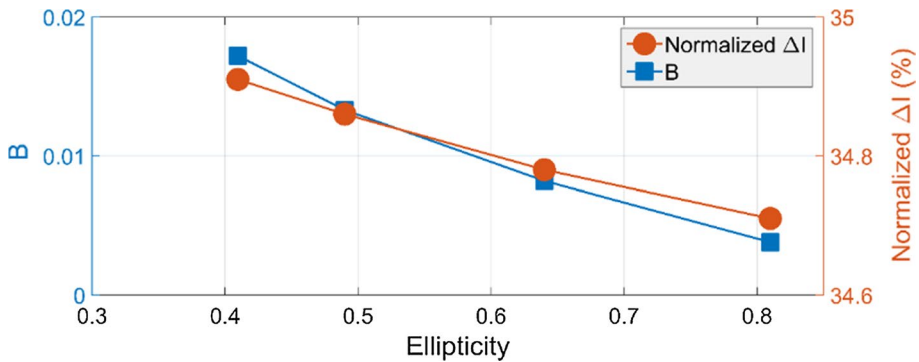


Fig. 6 Variation of B and normalized ΔI with the ellipticity for pitch $\Lambda=1.0$ μm of 3rd HB-IG-PCF shown in Fig. 3

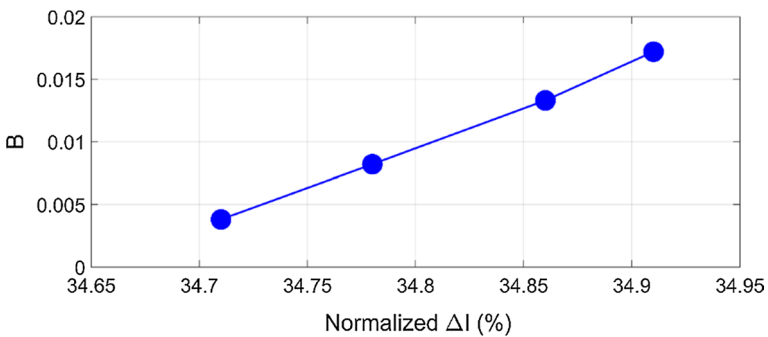


Fig. 7 Variation of B with normalized ΔI for pitch $\Lambda=1.0$ μm of 3rd HB-IG-PCF shown in Fig. 3

Furthermore, for the fourth HB-IG-PCF illustrated in Fig. 4, the variation of the phase birefringence B with the normalized difference of moments of inertia ΔI are shown in Fig. 8a–g, in detail. The parameters for the structure of HB-IG-PCFs in Fig. 8 are listed in the Table 2.

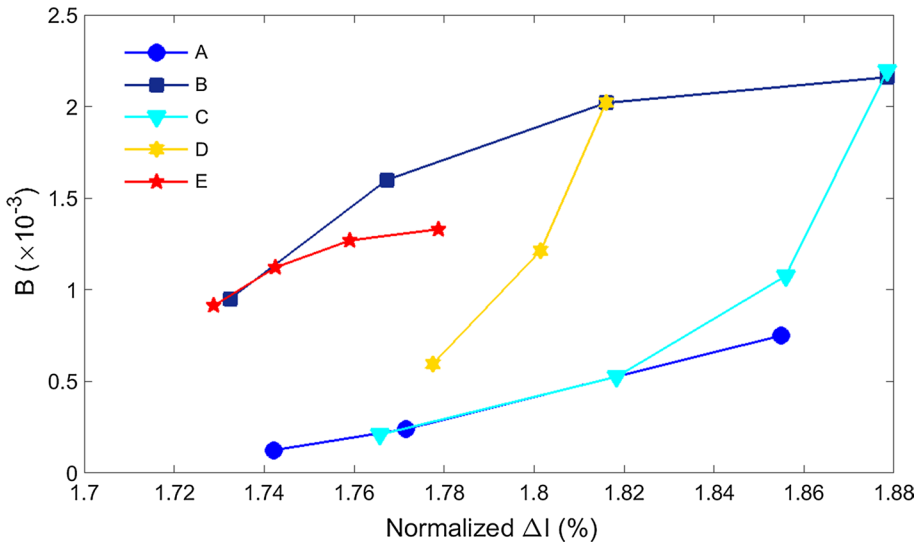


Fig. 8 Variation of B with ΔI for the 4th HB-IG-PCF shown in Fig. 4. The parameters are shown in Table 2

Table 2 Parameters for the structure of the 4th HB-IG-PCF as shown in Fig. 8

Legend	Parameters for the structure		
	a (μm)	b (μm)	Λ (μm)
A	0.6	1.0	2, 3, 4
B	$0.2 \cdot b$	0.4, 0.6, 0.8, 1.0	2.3
C	0.2, 0.4, 0.6, 0.8	1.0	2.3
D	0.2, 0.4, 0.6	0.8	2.3
E	$0.4 \cdot b$	0.4–1.1	2.3

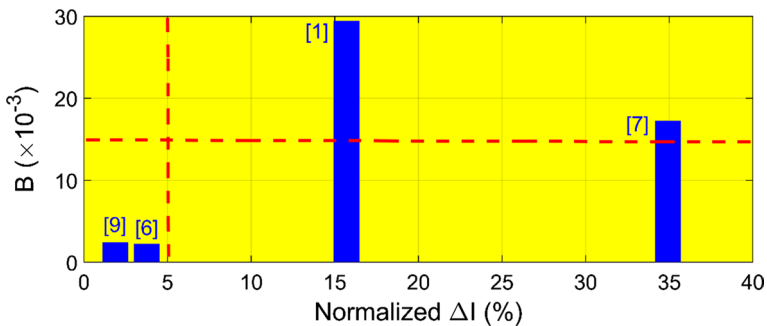
In various cases of changed Λ and constant a and b , changed a and b with constant pitch, and changed a with constant b and Λ , the phase birefringence B also increases monotonously when normalized ΔI rises.

We have found that the normalized difference of moments of inertia ΔI is effective to evaluate the structural anisotropy, which produces the geometric birefringence. For a certain PCF structure, it seems that in order to obtain the high B , optimizing the parameters of the structure to increase the normalized ΔI is an effective method.

Furthermore, the maximal B and normalized ΔI for four different HB-IG-PCFs are shown in the Table 3 and Fig. 9. As shown in Fig. 9, there are obviously two regions in the maximal B and normalized ΔI relationship: small normalized ΔI ($< 5\%$) and large normalized ΔI ($> 15\%$), where the maximal B is with the magnitude of 1×10^{-3} and 10×10^{-3} , respectively. Firstly, the relationship between the magnitude orders of normalized ΔI and B among different HB-IG-PCF structures is monotonicity. The larger normalized ΔI than 10% order: 15.71% of the 1st HB-IG-PCF structure (Habib et al. 2014a) and 34.91% of the 3rd structure (Liu and Lai 2005), there is a huge B in 10^{-2} order; and for the smaller normalized ΔI than 5% order: 3.75% of the 2nd HB-IG-PCF structure (Gangwar and Singh 2016) and 1.88% of the 4th HB-IG-PCF structure (Jiang et al. 2015), there is a remarkably small B in 10^{-3} order.

Table 3 The maximal B and normalized ΔI for four different HB-IG-PCFs

References	n_{silica}	n_{air}	λ (nm)	B_{max}	Normalized ΔI (%)
Habib et al. (2014a)	1.45	1	1550	29.4×10^{-3}	15.71
Gangwar and Singh (2016)	1.45	1	1550	2.2×10^{-3}	3.75
Liu and Lai (2005)	1.45	1	1550	17.2×10^{-3}	34.91
Jiang et al. (2015)	1.45	1	1550	2.4×10^{-3}	1.88

**Fig. 9** Variation of maximal B and normalized ΔI for four different HB-IG-PCFs as shown in Table 3

However, there is no strictly monotonous relationship between the normalized ΔI and B for different HB-IG-PCF structures with the same order of magnitude of normalized ΔI and B . Therefore, in the case of different HB-IG-PCF structures, other parameters that can describe the structural anisotropy more accurately and comprehensively must exist. We believe that there is a limitation of the quantitative describing the structural asymmetry by only one parameter (ΔI). It can not plenary and accurately describe the structural asymmetry, but can only reflect the cumulative effect of the structural asymmetry by the overall difference between the moment of inertia in x and y directions. There may be such a situation: the two optical fiber cross-section structures have the same shape and number of holes, but with the different distribution, however, there may be the same moment of inertia difference that can be obtained. Therefore, finding a parameter to quantitatively describe the structural asymmetry is indeed an open question. The undetermined parameters may be with clear physical meaning by defined or with only pure mathematical forms by machine learning, which will be focused in our future work.

5 Conclusion

In conclusion, we have investigated the structural anisotropy of four different HB-IG-PCFs, to find the essential factor to produce the geometric birefringence, quantitatively. In order to exclude the influences of other factors such as high-refractive-index nanostructures, four typical HB-IG-PCFs reported in the literatures are analyzed, with the same air and silica structure and 1550 nm wavelength, and circular, ellipse, and rectangle air holes.

Then, the normalized difference of moment of inertia is utilized to describe the structural anisotropy of HB-IG-PCFs. We have found that normalized ΔI is effective to evaluate the structural anisotropy, which produces the geometric birefringence. The phase birefringence B increases monotonously when normalized ΔI rises. In order to obtain high B for a PCF, it can be an effective method to optimize the parameters of the structure to increase the normalized ΔI . This work is a useful attempt to find the essence of geometric birefringence and bring a novel method to the study and design of PCFs, which will be the subject of a future work.

Acknowledgements This work is supported by the Fundamental Research Funds for the Central Universities (2018JBM070), the National Natural Science Foundation of China (Nos. 61675019, 61527822, and 61735005), the National Natural Science Foundation of Beijing (No. 4182054), Program for Changjiang Scholars and Innovative Research Team in University (Grant No. IRT_16R07), and the National Key R&D Program of China (2016YFC0800500).

References

- Brosi, J.M., Koos, C., Andreani, L.C., Waldow, M., Leuthold, J., Freude, W.: High-speed low-voltage electro-optic modulator with a polymer-infiltrated silicon photonic crystal waveguide. *Opt. Express* **16**(6), 4177–4191 (2008)
- Chen, D., Shen, L.: Highly birefringent elliptical-hole photonic crystal fibers with double defect. *J. Light-wave Technol.* **25**(9), 2700–2705 (2007)
- Chen, X., Li, M.J., Venkataraman, N., Gallagher, M.T., Wood, W.A., Crowley, A.M., Carberry, J.P., Zenteno, L.A., Koch, K.W.: Highly birefringent hollow-core photonic bandgap fiber. *Opt. Express* **12**(16), 3888–3893 (2004)
- Gangwar, R.K., Singh, V.K.: Study of highly birefringence dispersion shifted photonic crystal fiber with asymmetrical cladding. *Optik* **127**(24), 11854–11859 (2016)
- Habib, M.S., Khandker, E.: Highly birefringent photonic crystal fiber with ultra-flattened negative dispersion over S + C + L + U bands. *Appl. Opt.* **54**(10), 2786–2789 (2015)
- Habib, M.S., Habib, M.S., Hasan, M.I., Razzak, S.M.A.: Highly nonlinear polarization maintaining two zero dispersion spiral photonic crystal fiber using artificial defects. *Opt. Fiber Technol.* **19**(6), 539–542 (2013)
- Habib, M.S., Ahmad, R., Habib, M.S., Razzak, S.M.A.: Maintaining single polarization and dispersion compensation with modified rectangular microstructure optical fiber. *Optik* **125**, 4030–4034 (2014a)
- Habib, M.S., Habib, M.S., Hasan, M.I., Razzak, S.M.A., Hossain, M.A., Namihira, Y.: Polarization maintaining large nonlinear coefficient photonic crystal fibers using rotational hybrid cladding. *Optik* **125**(3), 1011–1015 (2014b)
- Halliday, D., Resnick, R., Walker, J.: *Fundamentals of Physics*, 9th edn. Wiley, New York (2013). ISBN 978-0-470-46908-8
- Hasan, M.I., Habib, M.S., Habib, M.S., Razzak, S.M.A.: Highly nonlinear and highly birefringent dispersion compensating photonic crystal fiber. *Opt. Fiber Technol.* **20**(1), 32–38 (2014)
- Hu, D.J.J., Shum, P.P., Lu, C., Ren, G.: Dispersion-flattened polarization-maintaining photonic crystal fiber for nonlinear applications. *Opt. Commun.* **282**(20), 4072–4076 (2009)
- Huang, T., Liao, J., Fu, S., Tang, M., Shum, P., Liu, D.: Slot spiral silicon photonic crystal fiber with property of both high birefringence and high nonlinearity. *IEEE Photonics J.* **6**(3), 1–7 (2014)
- Jiang, G., Fu, Y., Huang, Y.: High birefringence rectangular-hole photonic crystal fiber. *Opt. Fiber Technol.* **26**, 163–171 (2015)
- Knight, J.C.: Photonic crystal fibres. *Nature* **424**, 847–851 (2003)
- Li, P., Zhao, J.: Polarization-dependent coupling in gold-filled dual core photonic crystal fibers. *Opt. Express* **21**(5), 5232–5238 (2013)
- Liu, Y.C., Lai, Y.: Optical birefringence and polarization dependent loss of square- and rectangular-lattice holey fibers with elliptical air holes: numerical analysis. *Opt. Express* **13**(1), 225–235 (2005)
- Mousavi, S.A., Sandoghchi, S.R., Richardson, D.J., Poletti, F.: Broadband high birefringence and polarizing hollow core antiresonant fibers. *Opt. Express* **24**(20), 22943–22958 (2016)

- Saitoh, K., Koshiba, M.: Single-polarization single-mode photonic crystal fibers. *IEEE Photonic Technol. Lett.* **15**(10), 1384–1386 (2003)
- Samiul Habib, M., Nasim, K.M., Selim Habib, M., Hasan, M.I., Ahmad, R.: Relative dispersion slope matched dispersion compensating highly birefringent spiral microstructure optical fibers using defected core. *Opt. Eng.* **52**(9), 096110 (2013)
- Song, P., Zhang, L., Wang, Z., Hu, Q., Zhao, S., Jiang, S., Liu, S.: Birefringence characteristics of squeezed lattice photonic crystal fibers. *J. Lightwave Technol.* **25**(7), 1771–1776 (2007)
- Sun, Y.S., Chau, Y.F., Yeh, H.H., Shen, L.F., Yang, T.J., Tsai, D.P.: High birefringence photonic crystal fiber with a complex unit cell of asymmetric elliptical air hole cladding. *Appl. Opt.* **46**(22), 5276–5281 (2007)
- Szpułak, M., Statkiewicz, G., Olszewski, J., Martynkien, T., Urbanczyk, W., Wojcik, J., Makara, M., Klimek, J., Nasilowski, T., Berghmans, F., Thienpont, H.: Experimental and theoretical investigations of birefringent holey fibers with a triple defect. *Appl. Opt.* **44**(13), 2652–2658 (2005)
- Wei, S., Yuan, J.H., Yu, C.X., Wu, Q., Farrell, G., Li, S., Jin, B.Y., Hu, X.M.: Design on a highly birefringent and highly nonlinear tellurite ellipse core photonic crystal fiber with two zero dispersion wavelengths. *Opt. Fiber Technol.* **20**(4), 320–324 (2014)
- Xu, Q., Almeida, V.R., Panepucci, R.R., Lipson, M.: Experimental demonstration of guiding and confining light in nanometer-size low refractive-index material. *Opt. Lett.* **29**(14), 1626–1628 (2004)
- Yang, T., Wang, E., Jiang, H., Hu, Z., Xie, K.: High birefringence photonic crystal fiber with high nonlinearity and low confinement loss. *Opt. Express* **23**(7), 8329–8337 (2015)
- Yue, Y., Kai, G., Wang, Z., Sun, T., Jin, L., Lu, Y., Zhang, C., Liu, J., Li, Y., Liu, Y., Yuan, S., Dong, X.: Highly birefringent elliptical-hole photonic crystal fiber with squeezed hexagonal lattice. *Opt. Lett.* **32**(5), 469–471 (2007)
- Zhang, L., Yang, C.: Photonic crystal fibers with squeezed hexagonal lattice. *Opt. Express* **12**(11), 2371–2376 (2004)